Towards Forming Micro-Bubbles in Liquid Steel

Roderick Guthrie and Mihaiela Isac

Abstract Gas injection into liquid steel baths is widely practiced, ever since the early days of Bessemer's pneumatic steelmaking process. What has not been fully appreciated is the critical role of bubble sizes for delivering higher quality commercial steels than is presently possible. This was first proposed by Prof P. Hayes and his research group. Using a full-scale water model of a typical 4-strand Ladle-Tundish-Mold system, we demonstrate the potential advantages of modifying a typical ladle shroud, to generate microbubbles within the water flowing into the tundish. This is possible by taking advantage of high shear rates and turbulence kinetic energy available in that region. These microbubbles enhanced the removal of "micro-inclusions" (hollow glass microspheres) in the 5–50 micron size range, to the upper surface of the tundish. There, they were absorbed into an overlaying "slag" phase. Accompanying CFD studies confirmed that no microbubbles in the size range generated (500–900 μm), pass through the submerged entry nozzles into the moulds.

Keywords Micro-bubbles · Full-scale water model tundish · Computational fluid dynamics (CFD) · Aqueous particle sensor systems · Steelmaking

Introduction

Bubble formation in liquid metal systems is typically quite different from that in water, owing to much higher surface tensions, and the non-wetting conditions between liquid metals and the refractory systems used to contain them. Thus, when gas is introduced through a submerged porous plug into liquid steel, the bubbles formed will begin to coalesce on the non-wetting refractory surface, and spread

R. Guthrie (✉) · M. Isac
McGill Metals Processing Centre, McGill University, Montreal, QC, Canada
e-mail: Roderick.guthrie@mcgill.ca; rod@mmpc.mcgill.ca

M. Isac
e-mail: Mihaiela.isac@mcgill.ca

across it. This large bubble will then continue to grow, until the forces of surface tension attaching the growing hemisphere to the surface, are overcome by the buoyancy force. As such, typical bubbles forming on porous plugs are much larger than those observed in a water system, and are often in the spherical cap regime, versus the spherical, or oblate spheroidal regimes for water systems [1, 2]. However, bubbles forming in a cross flow situation is an entirely different matter, given stronger shearing flows within the ladle shroud. As such, this could be the best place to purposively form microbubbles, even though the bubbles we had produced within our gas-shrouded, full scale ladle shroud, had typically been 4–6 mm. in diameter in the past [3]. Recently, on asking whether microbubbles had ever been found in cast steel slabs at TATA steel, Ijmuiden, Dr Gert Abbel recalled that researchers had indeed observed tiny bubbles in their steel castings when characterising the performance of their new conventional slab caster, some twenty years ago [4]. These observations are shown in Fig. 1, where it had been concluded that tiny bubbles must have been responsible (Table 1).

Fortunately, their presence had no apparent effect on steel properties, since these cavities were sealed up, and disappeared, during substantial thermo-mechanical working and reduction in thickness to form strip products. Other companies have also reported on the presence of tiny bubbles in their cast product, so there can be no doubt that microbubbles can, and are, formed in liquid steel, and can enter the final cast steel slab.

Despite this, the conventional wisdom [e.g. Ref. 5] states that bubble sizes entering continuous caster moulds are in the 2–4 mm size range and rise to the surface, though no direct bubble size measurements have yet been possible to date. The bubbles are assumed to be the result of argon flooding of the joints at the intersections of the ladle shroud and the tundish nozzle, and/or the SEN's connection to the tundish. Both these locations are difficult to seal, on account of negative gauge pressures at the joints. Nevertheless, there can be no doubt that argon protection of the killed liquid steel is essential, in order to prevent re-oxidation of the steel, accompanied by the formation of millions of alumina particles entering the final cast product! So, for us, the quest is on! How can we

Fig. 1 Photograph of just one surface of a continuously cast Ti-SULC steel slab, showing spherical cavities corresponding to microbubbles. Sample sizes 3 mm x 40 mm x 65 mm
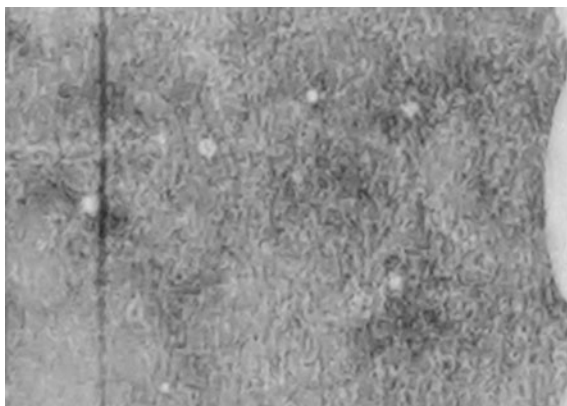
Table 1 Lists the relevant bubble size distributions determined for the five samples taken for a Titanium stabilised, ultra low carbon steel. The data reveals that many microbubbles in the 50–100 μm size range, plus the odd 500 μm bubble, had been detected within the slab's interior

Second Series of Microfocus Ti−SULC
Sample size: 3 mm x 40 mm x 65 mm
Bubble diameter

| μm	Nr. 8568	Nr. 8573	Nr. 8574	Nr. 8578	Nr. 8595
50–100	60	142	78	9	62
100–150	13	37	31	4	17
150–200	16	31	10	8	9
200–250	10	25	3	4	4
250–300	8	12	6	9	3
300–350	1	0	1	1	0
350–400	3	2	0	1	0
400–450	0	0	0	0	0
450–500	0	0	1	0	0
500–550	0	0	0	0	0
550–600	0	0	0	0	0
600–650	0	0	0	0	0
650–700	0	0	0	0	0
700–750	0	0	0	0	0
>750	0	1	0	0	0

design a ladle shroud, so as to produce only microbubbles of a selected size range within the ladle shrouds, and thereby "deep clean" liquid steel? To our knowledge, this concept was first reported in the literature by Professor Peter Hayes's research group in Brisbane, Australia [6]. Our work in this area, and further developments, are presented in this Symposium, celebrating Peter's accomplishments, and leadership, in High Temperature Process Metallurgy.

Water Models

The objective for our initial research was to gain a quantitative understanding of the mechanism of bubble generation under turbulent cross-flow conditions in a ladle shroud. Figure 2 shows a schematic of the initial experimental equipment that was assembled by X. Y. Ren [7], and used for measuring bubble sizes forming during side gas injection into his generic ladle shroud system.

As seen, a Turbine Water Flow Meter, plus a pressure gauge, were attached to the 21 mm diameter inlet pipe, located upstream of a metal nozzle slide gate system. Similarly, a Thermo Air Flow Meter was attached to the gas supply inlet ports, in order to prescribe the gas flowrate to the preselected nozzle. Three fixed slide gate openings could be chosen (Fully Open (100%), then 61.9%, and finally 23.8%).

Fig. 2 Experimental equipment for producing bubble streams and measuring bubble sizes
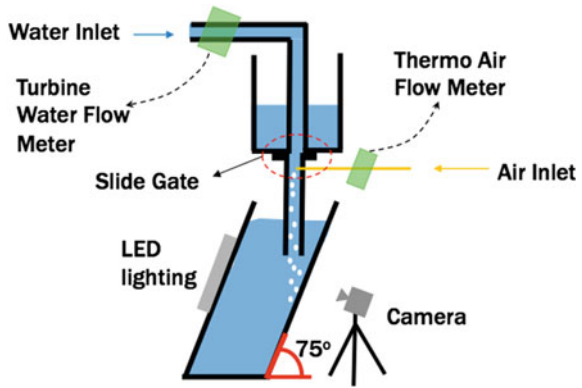
The dimensions matched the internal dimensions of the commercial, 4 strand billet caster, corresponding to our full scale water model of the complete ladle-tundish-mold system. See Fig. 3. To measure bubble sizes, we used the inclined rectangular tank, also depicted in Fig. 2. This allowed us to accurately observe and measure the many instantaneous monolayers of bubbles hitting the sidewall, so as to obtain a meaningful data set. A total of twelve data sets were needed, so as to determine the quantitative effects of the following variables; air flowrate, water speed, vertical

Fig. 3 View of water tank containing model tundish
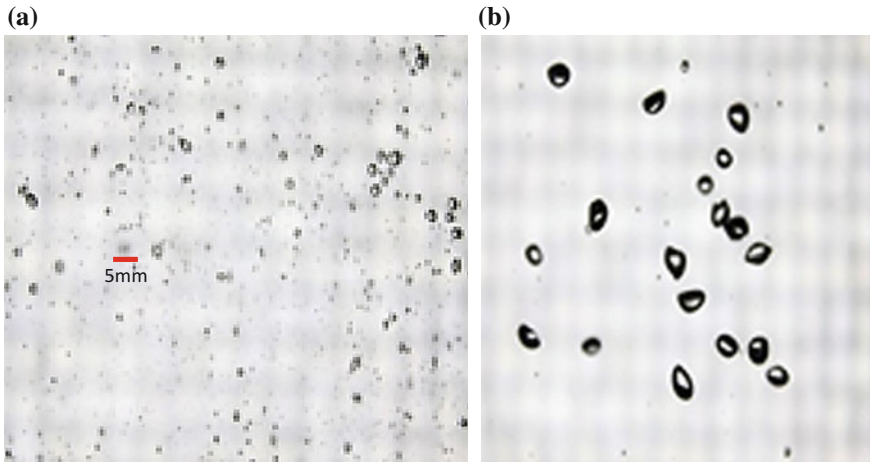
(a)　　　　　　　　　　　　　**(b)**

Fig. 4 Two regimes of bubble formation: **a** small bubbles less than 1 mm formed when the water speed is high and the air injection rate is low; **b** big bubbles >3 mm formed, when the water speed is low and the air injection rate is high

distance of injection orifice below the slide gate nozzle, opening ratio of the slide gate nozzle, and injection location. i.e. Front, Side, or Back of the ladle shroud.

We used a professional Digital Single-lens Reflex (DLSR) camera, Canon 50D, to capture bubble images shown in Fig. 4a and b. Professional photography level LED lights were installed on the back of the inclined tank, to provide consistent and bright light conditions. Figure 4a illustrates bubbles forming when the water speed is high, and the air flowrate is low, while Fig. 4b shows the bubbles forming when the water speed is low, and the gas flowrate is high.

To our delight, we had been able to create microbubbles in the ladle shroud without the need for any external measures or artefacts.

Following image processing using **Image J**, the extremely large data sets for each condition studied were statistically analysed, and the processed data would then be imported into a program called "Origin". With this system, X. Y. (Roger) Ren was able to summarize his findings in figures such as Fig. 5, where graphs of Bubble Count versus Bubble Diameter, for three different water speeds, for a specific set of conditions, is plotted. The three most important variables proved to be; (1) gas flow rate, (2) water speed, and (3) distance below the slide gate nozzle. The bubble size results are depicted as differently sized spheres in Fig. 6, where the ordinate(z) records % slide gate opening, the x abscissa records water inlet speed, and the y abscissa records inlet gas flowrate.

As seen, a smaller gas flowrate combined with a high water speed, and a small % slide gate opening, leads to small microbubbles being formed. We also see from Fig. 6, that bubbles were smaller, the closer they were to the orifice plate. With this knowledge, we then moved on to investigate the behaviour of microbubbles in the full scale water model tundish, fashioning a similar gas injection system for it, but with only three levels of gas injection ports close to the slide gate, as shown in Fig. 7.
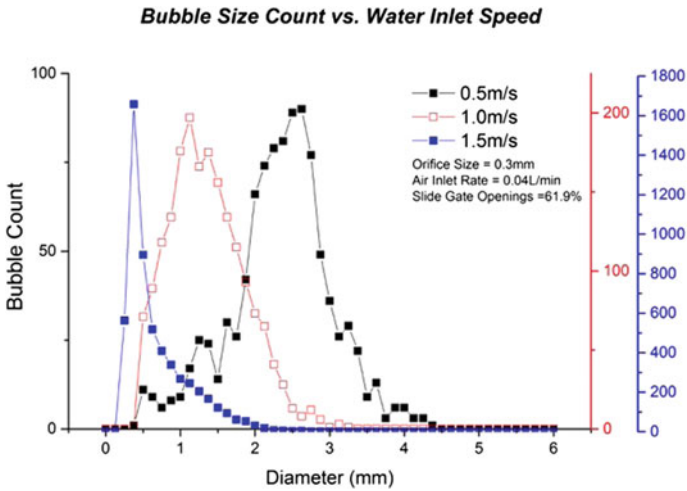
Bubble Size Count vs. Water Inlet Speed

Fig. 5 Bubble size versus water inlet speed, for single port, gas injection. Orifice size: 0.3 mm; Air inlet flowrate: 0.04L/min; Slide gate opening ratio: 61.9%; Position 1
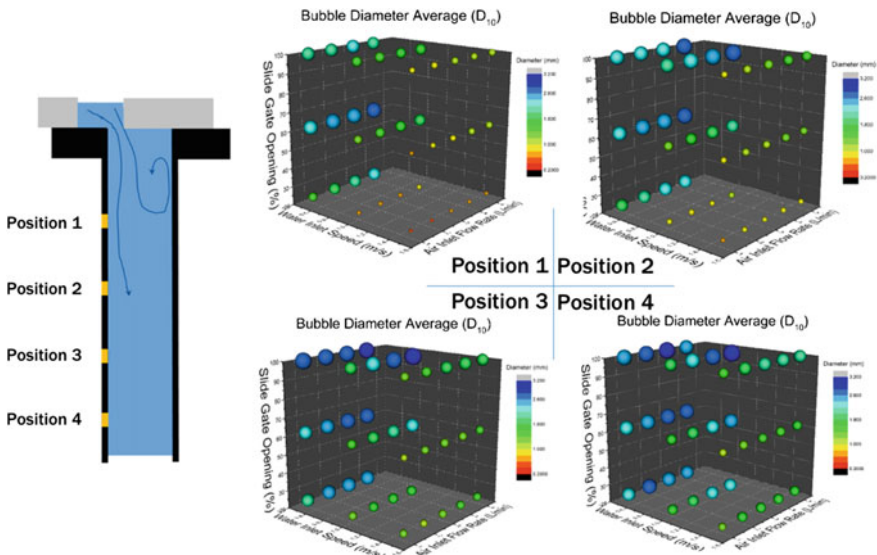

Fig. 6 Distance from the slide gate versus bubble size 0.5 mm orifice size, Front direction

We used a similar lighting arrangement and a submerged inclined plate to photograph bubbles impacting on the transparent plate, and were able to reproduce Ren's findings. See Fig. 8. In addition, we were also able to correlate the measured sizes of bubbles by photography, against those measured using the APS III bubble system, based on the ESZ (Electric Sensing Zone) principle. Up until about 800 μm
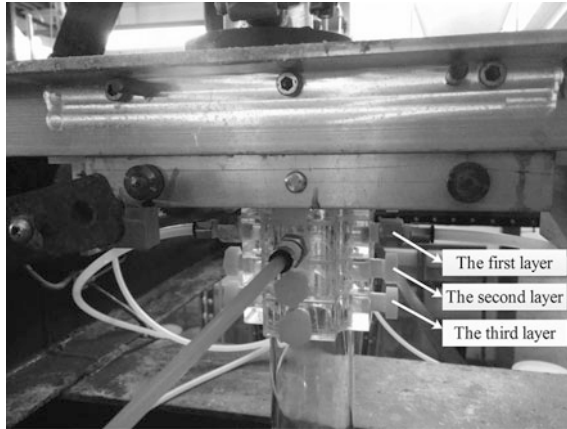
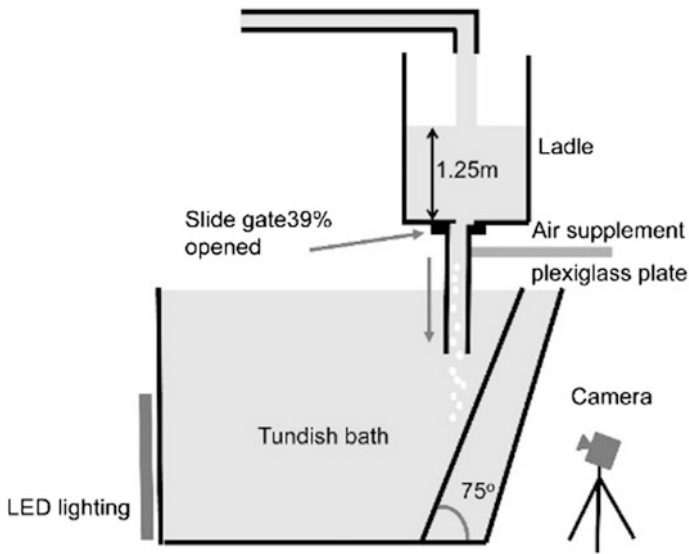**Fig. 7** Experimental microbubble dispenser

Fig. 8 Photo-measuring system for microbubble measurements in the full-scale ladle-tundish-mold

diameter bubbles, the correlation was excellent, but began to diverge at higher rising velocities.

This was expected, as some of the larger rising bubbles were not drawn into the ESZ, but escaped, causing a bias in the correlation. Finally, we introduced hollow glass microspheres into the ladle shroud, and measured the Residual Ratio of Inclusions (Amount of Inclusions entering exit ports to moulds/Amount of

Inclusions entering the tundish) in the presence, or not, of microbubbles, using the APS II inclusion system.

Aqueous Particle Sensor measurements of inclusion distributions, with and without, ladle "furniture", and the use of micro-bubbles.

The next step was to determine under what conditions the use of microbubbles can lead to the removal of inclusions in the less than 50 micron and below, size range. Towards that end, we have now established that a conventional ladle shroud, fitted with our first microbubble generator, is capable of removing 50% more inclusions of 23 micron diameter, and about 30% more inclusions of 32 microns in diameter, than was possible for a conventional tundish operation. This is shown in Fig. 9, reproduced from our article appearing in ISIJ [8]. Each condition was tested for a period of 30 s, with a baseline test used to determine the inherent noise pickup. An inclusion concentration of 25 g/L was used, having a maximum inclusion size of 75 μm, but with the majority of inclusions in the 30–40 micron size range.

Figure 10 compares the behaviour of very thin layers of simulated slag (~2 mm thick) being penetrated by microbubbles, versus thicker slag layers (~6 mm), being penetrated by typically larger bubbles of 4–6 mm, formed by injecting gas through a 3 mm orifice into the top of the ladle shroud, where the gas becomes dispersed into the water flowing through the ladle shroud.
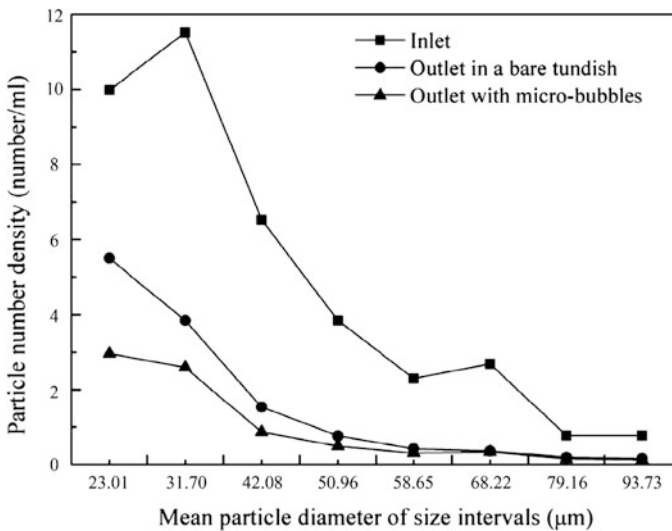

Fig. 9 Plot of particle number density of inclusions entering the RTIT tundish through the ladle shroud, versus the exiting flow number densities, in the presence, or not, of microbubbles [8]
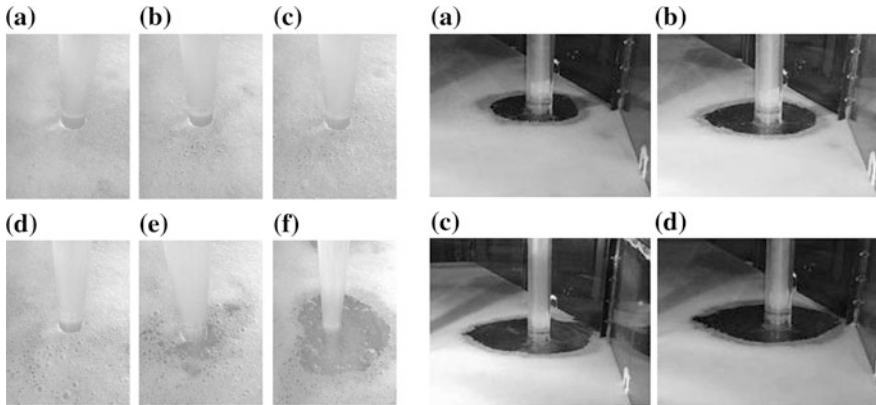
Fig. 10 Simulated slag behavior for microbubbles generated by one single port for gas injection, at gas flowrates of: **a** 0.1 L/min **b** 0.4 L/min, **c** 0.8 L/min, **d** 1.6 L/min. **e** 2.4 L/min, and **f** 3.8 L/min, compared to steel "eyes" that are formed for 2.4 L/min. gas flowrate [**a** = 2pct of water flow], and **b** 4%, **c** 6%, and **d** 10% of entering steel (water) flowrates

Mathematical Models

Using Fluent 14.5, a three-dimensional computational domain was established and meshed, using ICEM 14.5, into around 3.6 M hexahedral volume elements. We used our 288 core High Performance SGI computer cluster, operating at the MMPC, to solve the continuity and momentum equations, plus the k-ε equation for simulating the effects of turbulence, and the particle trajectory equation (so-called DPM) for representing particle (micro-bubble) movements within the computed flow system. To take into account the effect of turbulence in affecting the dispersion of microbubbles, the discrete random walk model was adopted. Once the steady state flow field was established, the bubbles began to be injected from the inlet surface, as the discrete phase. Simultaneously, the solution was changed to a time-dependent solution, using a fixed time step of 1 ms. Finally, the likelihood of particles becoming attached to rising microbubbles was based on the probability ($P = P_c P_a$ (%)) of attachment, as determined by Zhang and Taniguchi [9].

Results and Discussion

Figure 11 shows computational results for bubble trajectories for 3 mm size bubbles, versus 0.845 mm size bubbles.

It is clear that the larger 3 mm bubbles will rise back to the surface around the incoming jet stream. This will disrupt the overlying slag layer, and result in re-oxidation of killed steel, immediately around the ladle shroud, in keeping with previous observations. However, for smaller bubbles, of 0.845 mm diameter,
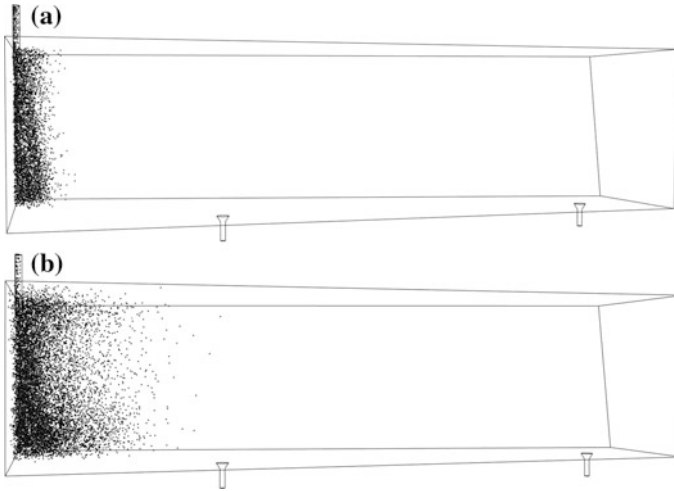
Fig. 11 Bubble distributions for different sizes: **a** 3 mm in diameter, **b** 0.845 mm in diameter

the bubbles will spread out, following the liquid flows more closely down along the tundish, thereby reducing the tendency to form a reverse flow recirculation zone around the ladle shroud [11, 12]. In this manner, ever smaller microbubbles will become ever more dispersed, and will also rise ever more slowly towards the surface. In the limit, microbubbles can become so small, that they will follow the liquid flow, and enter the SEN's. To avoid this, there will be an ideal microbubble size for a given tundish configuration and processing conditions, such that they can maximise the capture of the smaller particle remaining within the steel flow (i.e. in the 50 μm size range and below), without themselves becoming entrained within the exiting flows to the moulds. As noted before, this could lead to a step change in the quality of steel being sent to the moulds for solidification of the refined steel liquid.

Figure 12 shows the experimental diameters of microbubbles obtained in the present work, versus those predicted on the basis of a semi-empirical equation derived by Marshall et al. [10]. Their study of bubble formation in the horizontal crossflow of water lead to the equation;

$$R_b = 0.48\,R^{0.826}\left(U_{air}/U_{liquid}\right)^{0.36} \text{ where } U_{air} = Q_{air}/\pi R_{orifice}^2$$

As seen, there is an almost perfect 1:1 correlation, apart from a significant number of bubble sizes recorded that were somewhat lower. We believe that these were due to a second mechanism at work. Thus, for the 23.8% slide gate opening (black square dots in Fig. 12), there were usually strong spatial velocity variations, as shown in Fig. 13.

Fig. 12 Comparison of experimental bubble sizes versus predictions, using Eq. 1 for the cross-flow of water in a tube into which gas could be injected
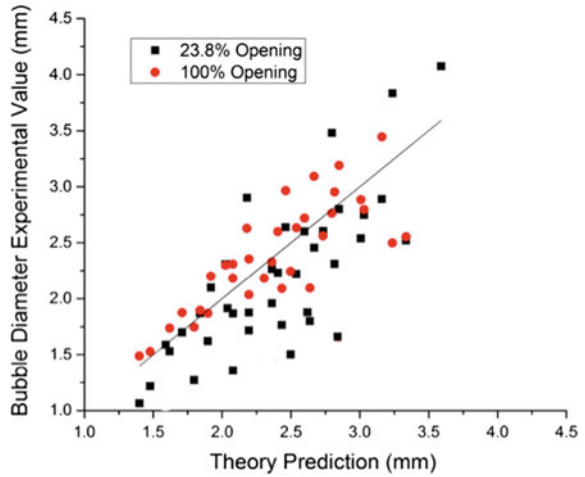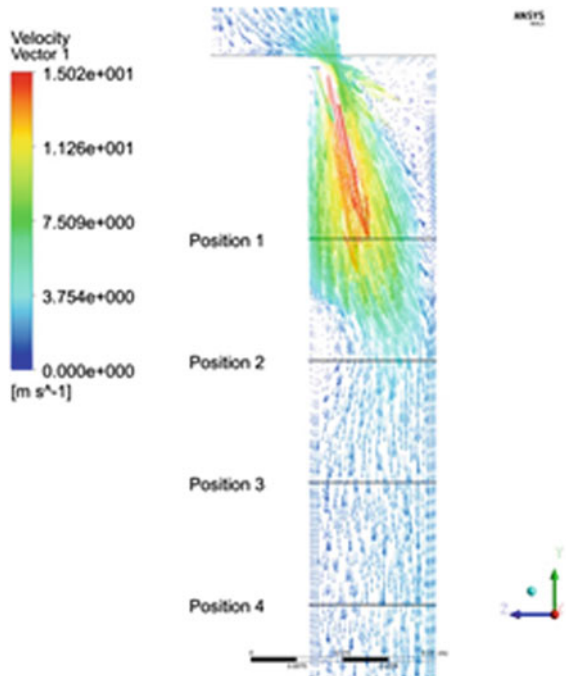

Fig. 13 Predicted local velocities close to the slide gate nozzle

This leads to the production of strong kinetic energy of turbulence and an associated high rate of dissipation of this kinetic energy of turbulence. We can conclude that the smaller bubbles were the result of subsequent break-up processes after being formed. It also explains our findings that injection distance below the slide gate nozzle, leads to larger bubble sizes.

Conclusions

This work has laid the foundations needed for producing, and measuring, microbubble sizes in liquid metal flow systems of interest to the steel industry. We show a methodology whereby both forming, and final, bubble sizes can be accurately measured and correlated against theoretical, or semi-empirical, data, and applied to a full scale water model system. The next step in this work will be to carry out equivalent flows in liquid metal/ceramic or refractory systems, so as to confirm, or not, equivalence of results under the much higher surface tensions of liquid steel systems. If so, refractory suppliers and steel companies will need to more precisely control argon gas flows into ladle shrouds, to ensure fully developed, single phase flows through their ladle shrouds. This will allow us to then determine whether the tentatively observed benefits in removing smaller inclusions <50 μm from steel, can translate into far higher quality steels in the future.

References

 1. Irons GA, Guthrie RIL (1978) Met Trans B 9(2):101–110
 2. Harris R, Ng KW, Wraith AE (2005) Chem Eng Sci 60(11):3111–3115
 3. Chattopadhyay K, Isac M, Guthrie RIL (2011) ISIJ Int 51(4):459–468
 4. Abbel G (2016) Private communication. TATA Steel, Ijmuiden
 5. Zhang LF, Aoki J, Thomas BG (2006) Metall Mater Trans B 37B:361
 6. Wang L, Lee H, Hayes P (1996) A new approach to molten steel refining using fine gas bubbles. ISIJ 36(1):17–24
 7. Ren XY (2015) Mechanical Engineering thesis, McGill University, Montreal, QC
 8. Chang S, Cao X, Hsin C-H, Zou Z, Isac M, Guthrie RIL (2016) Removal of inclusions using micro-bubble swarms in a four strand, full scale, water model tundish. ISIJ Int 56(7): 1188–1197
 9. Zhang LF, Taniguchi S (2000) Int Mater Rev 45:59–82
10. Marshall SH, Chudacek MW, Bagster DF (1992) Chem Eng Sci 47:3265–3272